# Approximation Method for the Calculation of Stress Intensity Factors for the Semi-elliptical Surface Flaws on Thin-Walled Cylinder

**Changheui Jang***

*Department of Nuclear and Quantum Engineering,*
*Korea Advanced Institute of Science and Technology,*
*373-1 Guseong-dong, Yuseong-gu, Daejeon 305-701, Korea*

A simple approximation method for the stress intensity factor at the tip of the axial semi-elliptical cracks on the cylindrical vessel is developed. The approximation methods, incorporated in VINTIN (Vessel INTegrity analysis-INner flaws), utilizes the influence coefficients to calculate the stress intensity factor at the crack tip. This method has been compared with other solution methods including 3-D finite element analysis for internal pressure, cooldown, and pressurized thermal shock loading conditions. For these, 3-D finite-element analyses are performed to obtain the stress intensity factors for various surface cracks with $t/R$=0.1. The approximation solutions are within ±2.5% of the those of finite element analysis using symmetric model of one-forth of a vessel under pressure loading, and 1-3% higher under pressurized thermal shock condition. The analysis results confirm that the approximation method provides sufficiently accurate stress intensity factor values for the axial semi-elliptical flaws on the surface of the reactor pressure vessel.

**Key Words :** Stress Intensity Factor, Thin-Walled Cylinder, Influence Coefficient, Semi-elliptical Flaws, Finite Element Analysis

## 1. Introduction

Because of the close proximity to the reactor core, the beltline region of the reactor pressure vessel (RPV) of the nuclear power plant (NPP) is subjected to the irradiation embrittlement caused by the fast neutron exposure during operation, resulting in reduced fracture toughness. If flaws exist in the embrittled RPV, they are likely to propagate through the wall under severe transient conditions such as pressurized thermal shock (PTS) (USNRC, 1982). For the integrity assessment of the PTS, rather detailed fracture mechanics analyses are required. In the fracture mechanics analyses, the applied stress intensity factors (SIF) at the tip of the hypothetical flaws are compared with the materials fracture toughness to judge the stability of the flaws during the transient (Simonen et al., 1986). Therefore, accuracy of the SIF calculation for the ranges of the flaw shapes and depths during the transients are crucial for the fracture mechanics analyses.

Usually, the beltline region of the RPV is treated as an infinite cylinder during thermal and stress analyses and SIF calculation because it is sufficiently far away from nozzles and heads. Both the direct and indirect methods can be used to calculate the SIF at the tip of the flaws in the beltline region of the RPV. The typical direct method is the finite element method (FEM), in

* Corresponding Author,
**E-mail** : chjang@kaist.ac.kr
**TEL** : +82-42-869-3824; **FAX** : +82-42-869-3810
Department of Nuclear and Quantum Engineering, Korea Advanced Institute of Science and Technology, 373-1 Guseong-dong, Yuseong-gu, Daejeon 305-701, Korea. (Manuscript **Received** August 5, 2005; **Revised** January 28, 2006)

that the 3D finite element model of the flaws are used to calculate the J-integral values which in turn are converted into the SIF values (Kim et al., 2001). Despite of the high accuracy of the results, the modeling and analysis have to be repeated once the flaw shape or depth changes even for the same transients.

In the typical indirect methods, the SIF at the tip of the flaws are calculated using the stress distribution within the structure without flaws and the pre-determined influence coefficients. In this case, once the influence coefficient database for the ranges of flaw shapes and depths are established, only the stress analyses are repeated to calculate the SIFs for different transients. The Raju-Newman's method (Raju and Newman, 1982) and ASME Sec. XI App. A method (ASME, 1995) are the typical examples of the indirect methods. The Raju-Newman's method has been widely used to calculate the SIFs for fracture mechanics analyses. Raju-Newman calculated influence coefficients for ranges of semi-elliptical flaws in infinite cylinder with thickness to radius ($t/R$) ratio of 0.1 and 0.25. They used 1/8 symmetric finite element model of axial inner surface flaws and stress distribution approximated as 3-rd order polynomials to determine the influence coefficients.

An approximation method using the Raju-Newman's influence coefficients to find SIFs for inner surface flaws in nuclear reactor pressure vessel was developed and incorporated into the probabilistic fracture mechanics code for PTS integrity analysis, VINTIN (Vessel INTegrity INner flaws) (Jang et al., 2001a). The accuracy of the method was compared with the FAVOR code (Dickson, 1994) developed by USNRC (Jang et al., 2000). Also, the analysis results were benchmarked with the detailed FEM analyses for various thermal and pressure loading conditions (Moon and Jang, 2001 ; Jang et al., 2001b).

In this paper, the VINTIN approach for SIF calculation are explained and compared with other methods as an effort to verify the appropriateness of the VINTIN code. The calculated SIFs using approximation method for various loading conditions are compared with the detailed FEM results using ABAQUS.

## 2. Methods for SIF Calculation

### 2.1 J-integral using FEM

J-integral values are used to calculate the SIFs for the flaws in cylinder. J-integral is defined as follows ;

$$J=\int_{\Gamma}\left(Wdy-T_i\frac{\partial u_i}{\partial x}ds\right) \tag{1}$$

where, $\Gamma$ is the arbitrary integration path in displacement field in counterclockwise direction, $T_i$ is the outward normal stress vector on $\Gamma$, $U_i$ is the displacement vector, $ds$ is the infinitesimal length on integration path, and $W$ is the strain energy density represented by the following equation.

$$W=\int_0^{\varepsilon}\sigma_{ij}d\varepsilon_{ij} \tag{2}$$

For J-integral calculation, several finite element analysis tools are available, including ABAQUS code. Mathematically, J-integral is path-independent, and same as the energy release rate $G$ in elastic regime. In this paper, the area integration method proposed by Shih et al.(1986) is used to calculated J-integral, which in turn is used to find SIFs, or $K$ from the following equation.

$$K=\sqrt{\frac{EJ}{(1-v^2)}} \quad \text{for plane strain} \tag{3}$$

### 2.2 Raju-newman method

Though the FEM gives fairly accurate results of SIFs, it take fair amount of time for modeling and analysis. Furthermore, the effects of different finite element model and analysis scheme are usually non-negligible for most cases. Also, because the analyses results are applicable only for the specific flaw shape, location, and depth, new analyses are required as the flaw characteristics are altered. In this respect, the direct use of FEM analysis for the PFM analysis for PTS, in that the flaw aspect ratio and depth are treated as distributed function, and $K$ at various flaw depth are needed, is practically impossible. To cope with the problem, the indirect method like Raju-Newman method is incorporated in various PFM

code for PTS analysis (Raju and Newman, 1982). The Raju-Newman method is summarized as follows;

The stress distribution within the infinite cylinder can be fitted as 3-rd order polynomials as follows;

$$\sigma=\sum_{j=0}^{3} A_j x^j=\sum_{j=0}^{3} A_j a^j \left(\frac{x}{a}\right)^j \tag{4}$$

where, $x$ is the distance from the inner surface of the cylinder, $a$ is the depth of the flaws. For the stress distribution given as Eq. (4), SIF at the tip of the flaw can be calculated by the Eq. (5) given below.

$$K=\sqrt{\frac{\pi a}{Q}}\sum_{j=0}^{3} G_j A_j a^j \tag{5}$$

where

$G_j$=influence coefficient
$A_j$=coefficient of the stress distribution given as Eq. (4)
$Q$=geometry factor
$=1+1.464\left(\frac{a}{c}\right)^{1.65}$
$c$=length of the flaw

### 2.3 ASME Sec. XI method

ASME Sec. XI App. A procedure is similar to Raju-Newman method. But the stress distribution is fitted with $x/a$ instead of $x$. SIF at the tip of the flaw can be calculated by the Eq. (7) given below.

$$\sigma=\sum_{j=0}^{3} B_j \left(\frac{x}{a}\right)^j \tag{6}$$

$$K=\sqrt{\frac{\pi a}{Q}}\sum_{j=0}^{3} G_j B_j \tag{7}$$

where

$B_j$=coefficient of the stress distribution given as Eq. (6)

Though Eq. (7) looks similar to Eq. (5) of the Raju-Newman method, the influence coefficients in ASME Sec. XI App. A procedure are those for the semi-elliptical flaws in infinite plate, while those in Eq. (5) are for the semi-elliptical flaws in infinite cylinder.

### 2.4 Approximate method in VINTIN

In VINTIN code, the temperature distribution is found by numerical method, and the thermal stress distribution is calculated from the temperature distribution. The hoop stress from internal pressure is calculated separately from the analytic solution. Then each stress distribution is approximated as 3-rd order polynomial as follows.

$$\sigma=\sum_{j=0}^{3} C_j \left(\frac{x}{t}\right)^j \tag{8}$$

where

$C_j$=coefficient of the stress distribution given as Eq. (8)

It should be noted that the stress distribution is shown as function of the distance from the inner surface normalized with the thickness of the cylinder. For the stress distribution of Eq. (8), SIF at the tip of the flaw can be calculated by the Eq. (9) given below.

$$K=\sqrt{\frac{\pi a}{Q}}\sum_{n=0}^{3} G_n C_n \left(\frac{a}{t}\right)^n \tag{9}$$

Raju-Newman provided the influence coefficients for axial semi-elliptical flaws on the inner surface of the infinite cylinder of thickness to radius ratio $(t/R)$ of 1/10 for several flaw shapes and depths using FEM results on the 1/8 symmetric flaw models. Wu-Carlsson provided those for axial infinite flaws in the same geometry (Wu and Carlsson, 1991). VINTIN code (Jang et al., 2000) uses these published results and fitted them to find the influence coefficients for wide ranges of flaw shape and depth, or aspect ratio $(a/c)$ of 1.0 (semi-circular) to 0 (infinite) and normalized depth $(a/t)$ of 0 to 1. The equations bellow are examples of the fitted formula for the semi-elliptical flaws with aspect ratio $(a/c)$ of 0.4.

$$\begin{aligned}
G_0&=1.079-0.3504(a/t)\\
&\quad+1.7931(a/t)^2-1.0806(a/t)^3\\
G_1&=0.667-0.0470(a/t)\\
&\quad+0.3882(a/t)^2-0.1403(a/t)^3\\
G_2&=0.499+0.1597(a/t)\\
&\quad-0.2514(a/t)^2+0.2639(a/t)^3\\
G_3&=0.410+0.2385(a/t)\\
&\quad-0.5007(a/t)^2+0.4153(a/t)^3
\end{aligned} \tag{10}$$

The advantage of the VINTIN approach is that the stress distributions are represented as the distance normalized to the thickness of the cylinder, and, therefore, the same stress coefficient can be used in Eq. (9) to calculate the SIF for various flaw depths. Whereas, the stress coefficients have to be recalculated if the flaw depth are changed in Raju-Newman and ASME Sec. XI methods.

## 3. Analysis Conditions and FEM Model

### 3.1 Geometry and conditions

The reactor pressure vessel considered in the analysis is 2,184 mm inner radius and 216 mm thick. Stainless steel clad is not considered. The thermo-physical properties of the RPV materials are summarized in Table 1. Fig. 1 shows the schematic of the cylinder. Thickness to radius ratio $(t/R)$ of the cylinder is 0.1. The flaws assumed are semi-elliptical inner surface flaws with length of $2c$ and depth of $a$. The length of the cylinder is calculated from the radius to minimize the end effect (Timoshenko, 1940).

The loading conditions and main areas of investigation are as follows;

(1) Internal pressure of 15.5 MPa: compare the FEM results of 1/4- and 1/8-symmetric flaw model with those of approximation methods.

(2) Fast cooling condition in which the coolant temperature exponentially decreases from 287.8℃ to 51.7℃ following the equation of $T=51.7+236.1\cdot\exp[-0.05\,t(\text{min})]$: compare the FEM results of 1/4-symmetric flaw model with those of approximation methods.

(3) PTS transient condition in which above two conditions occur simultaneously: compare the FEM results of 1/4-symmetric flaw model with those of VINTIN methods.

The heat transfers in thickness direction only, and the outer wall is insulated. The heat transfer coefficient on the inner surface is assumed at 1,704 $W/m^2$-℃ for the thermal transient considered in this analysis.

**Table 1** Thermo-physical properties of the reactor pressure vessel materials

| Material Property | Values |
|---|---|
| Thermal Conductivity, W/m-℃ | 40.89 |
| Specific Heat, J/Kg-℃ | 509.14 |
| Density, $Kg/m^3$ | 7809.2 |
| Modulus of Elasticity, GPa | 177.0 |
| Thermal Expansion Coefficient, m/m-℃ | 13.21E-6 |
| Poisson's Ratio | 0.3 |

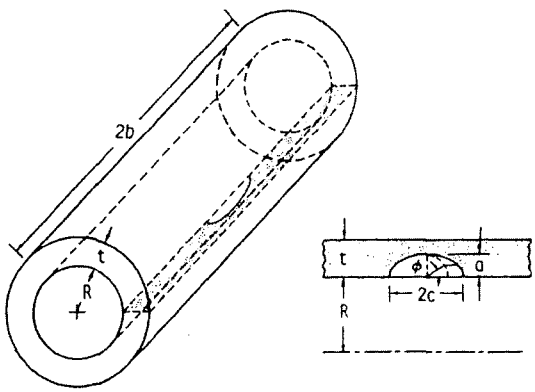


**Fig. 1** Schematic of the internal semi-elliptical surface crack in a infinite cylinder

### 3.2 Finite element model

For FEM analysis, ABAQUS is used. The element used is 20-node quadratic iso-parametric quadratic brick element with reduced integration. Fig. 2 shows the 1/4-symmetric flaw model of the cylinder used in the analysis. The 1/8-symmetric

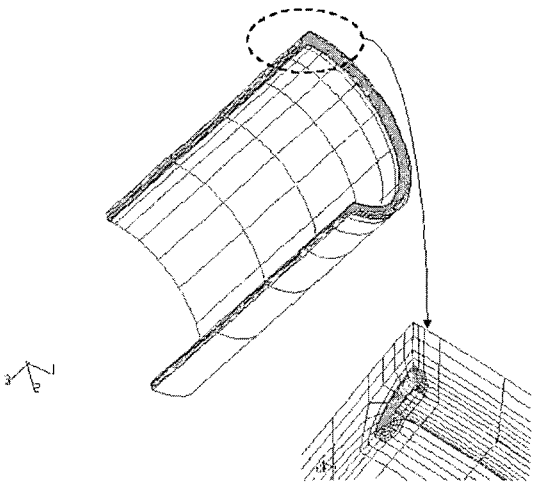

**Fig. 2** Details of a typical finite element mesh for symmetric one-fourth of a vessel

model is similar to this but encompass 90 degree in azimuthal angle. The degree of freedom of the model is 28,935. To investigate the effects of the symmetric models, both 1/4- and 1/8-symmetric models are used for internal pressure condition. But for conditions 2) and 3), only the 1/4-symmetric model is used. The symmetric planes are fixed in the direction normal to the plane and free to move in other two directions. In 1/4-symmetric model, a node on the $r-\theta$ plane is constrained to prevent parallel motion.

Using the FEM models, SIFs at the tip of the flaws are calculated from the J-integral using area integration. J-integral values for 6 paths near the tip of the flaw tip are calculated. J-integral value nearest to the flaw tip is excluded, and the remaining 5 J-integral values are averaged to calculate the path-independent J-integral for the given flaws shape and depth. The differences among the 5 J-integral paths are less than 1%. The path-independent J-integrals are converted to SIF, or K using Eq. (3) for plane strain condition.

For loading condition 1), flaw shape and depth are varied as shown in Table 2. The flaws with $a/c$ of 0.2 and 0.4, $a/t$ of 0.2 and 0.5 are included to compared the results of Raju-Newman. Additionally, smaller flaws ($a/t$=0.059 and 0.118) with $a/c$ of 1/3 are included. Therefore, both 1/4- and 1/8-symmetric flaw models for 6 flaw shape and depth are analyzed.

For loading condition 2), flaw aspect ratio is fixed at $a/c$=2/5, and the $a/t$ is changed from 0.05 to 0.4 as shown in Table 3. The aspect ratio is selected to compare the Raju-Newman and ASME Sec. XI methods with VINTIN method.

For loading case 3), only flaw with $a/c$=2/5 and $a/t$=0.2 is analyzed for comparison.

**Table 2** The matrix for loading condition 1)

| crack depth to crack length ($a/c$) | Case | Crack depth ($a$) | | Crack length ($c$), mm |
|---|---|---|---|---|
| | | $a/t$ | $a$, mm | |
| 1/3 | 1-1 | 0.059 | 12.7 | 38.1 |
| | 1-2 | 0.118 | 25.4 | 76.2 |
| 1/5 | 1-3 | 0.2 | 43.2 | 216 |
| | 1-4 | 0.5 | 108 | 540 |
| 2/5 | **1-5** | **0.2** | **43.2** | **108** |
| | 1-6 | 0.5 | 108 | 270 |

**Table 3** Aspect ratio and $a/t$ of the flaws considered for loading condition 2)

| crack depth to crack length ($a/c$) | Case | Crack depth ratio, $a/t$ | Crack depth, $a$, $mm$ |
|---|---|---|---|
| 2/5 | 2-1 | 0.05 | 10.8 |
| | 2-2 | 0.1 | 21.6 |
| | **2-3** | **0.2** | **43.2** |
| | 2-4 | 0.25 | 54.0 |
| | 2-5 | 0.4 | 86.4 |

## 4. Results and Discussion

### 4.1 Effects of flaw model under internal pressure loading condition

In Table 4, SIFs from several approximate solutions are compared with those from FEM

**Table 4** Comparison of stress intensity factor from FEM analysis, Raju-Newman's and VINTIN calculation for internal surface crack

| Method / Case | Numerical method,% | | | | 3D-finite element method, % |
|---|---|---|---|---|---|
| | $(V-K_{1/8})/K_{1/8}$ | $(R-K_{1/8})/K_{1/8}$ | $(V-K_{1/4})/K_{1/4}$ | $(R-K_{1/4})/K_{1/4}$ | $(K_{1/4}-K_{1/8})/K_{1/8}$ |
| 1-1 | −8.95% | | 2.35% | | −11.03% |
| 1-2 | −8.71% | | −0.44% | | −8.31% |
| 1-3 | −8.44% | −9.59% | −0.43% | −1.68% | −8.05% |
| 1-4 | −6.70% | −7.93% | −2.36% | −3.65% | −4.44% |
| **1-5** | **−7.30%** | **−8.44%** | **0.37%** | **−0.87%** | **−7.64%** |
| 1-6 | −3.21% | −4.42% | 0.84% | −0.42% | −4.02% |

V : VINTIN approximation
R : Raju-Newman solution
$K_{1/4}$ : 1/4 symmetric FEM solution
$K_{1/4}$ : 1/8 symmetric FEM solution

analysis for internal pressure loading conditions. As shown in the last column of the table, SIFs for 1/4-symmetric flaw models are about 4 to 11% smaller than those of the 1/8-symmetric flaw models in which two flaws are separated by 180 degree. The differences are somewhat greater than 2 to 4% proposed by Raju-Newman using the FEM model of low degree of freedom (Raju and Newman, 1982). The differences become larger as the flaw depth decreases.

In the third column of the table, SIFs from 1/8-symmetric flaw models are compared with those using Raju-Newman's method in which influence coefficients based on the 1/8-symmetric flaw models are used. Compared with Raju-Newman's methods, current study uses the degree of freedom of about 4 times and shows about 4 to 10% larger SIFs. Wang and Lambert (Wang and Lambert, 1996) used FEM model with degree of freedom of about 20,000 for 1/8-symmetric flaw model and reported about 6 to 8% higher influence coefficients than those proposed by Raju-Newman. They argued that the high degree of freedom contributed the increase in the influence coefficients. Because of the low degree of freedom used in Raju-Newman's study, the SIFs using influence coefficients for 1/8-symmetric flaws proposed by them are closer to the results of 1/4-symmetric flaw models with increased degree of freedom. It is clear when the third and the fifth columns of the table are compared.

In the second and fourth columns of the table, the approximate solution using VINTIN code are compared with the FEM results. In general, VINTIN code gives similar, but about 1% larger SIFs than Raju-Newman method. It seems that the difference in polynomial approximation of the stress distribution causes this, considering both VINTIN and Raju-Newman method uses the same influence coefficient. Though VINTIN code uses the influence coefficients from 1/8-symmetric flaw models, the SIFs calculated by it agree well (within ±2.5%) with those from 1/4-symmetric flaw model in this study.

The SIFs are plotted for aspect ratios in Figures 3 to 5. For all 3 aspect ratio considered in this study, 1/4-symmetric flaw model, Raju-Newman method, and VINTIN method show similar SIFs. This implies that the Raju-Newman and VINTIN methods can be applied to find reasonably accurate SIFs when the number of flaw along the perimeter of the cylinder is one. Or,

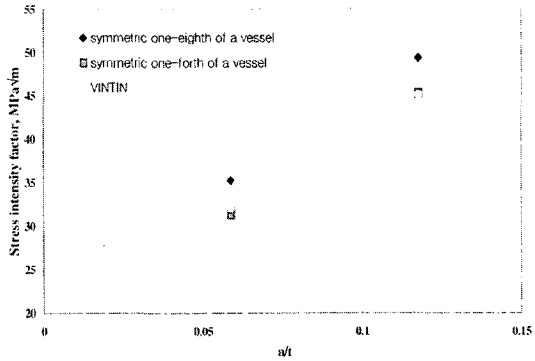


**Fig. 3** Comparison of stress intensity factors, for $a/c=1/3$, internal surface crack

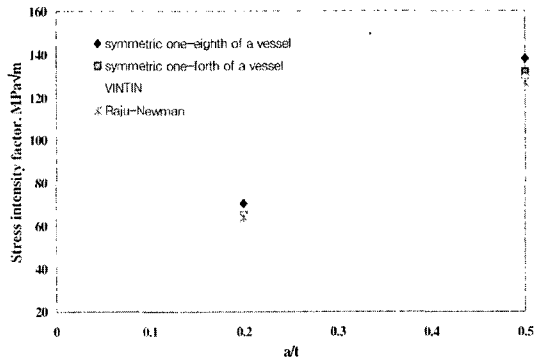


**Fig. 4** Comparison of stress intensity factors, for $a/c=2/5$, internal surface crack

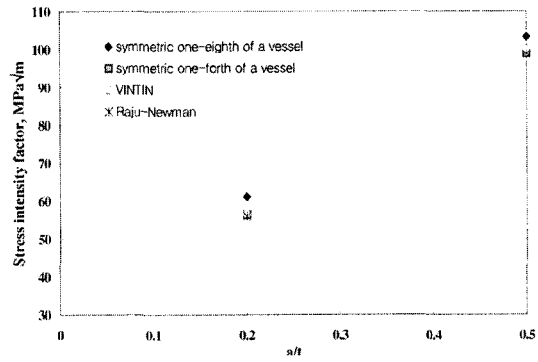


**Fig. 5** Comparison of stress intensity factors, for $a/c=1/5$, internal surface crack

they will underestimate SIFs if more than 2 flaws exist along the perimeter.

From the analysis for internal pressure loading condition, we find that the results of Raju-Newman's 1/8-symmetric flaw model are similar to those of 1/4-symmetric flaw model in this study. This is due to the low degree of freedom in Raju-Newman's model. Also, VINTIN method, in which Raju-Newman's influence coefficients are adopted, provide similar SIFs to 1/4-symmetric flaw model in this study.

### 4.2 Approximation methods under fast cooling condition

#### 4.2.1 Stress distribution

Figure 6 shows the stress distribution within the cylinder for loading condition 2). The stress distribution is the steepest at 1200 and 2400 seconds, then become modest as the heat transfer/conduction progress afterward. As shown in the figure, the stress distributions from VINTIN code agree well with those from FEM analysis.

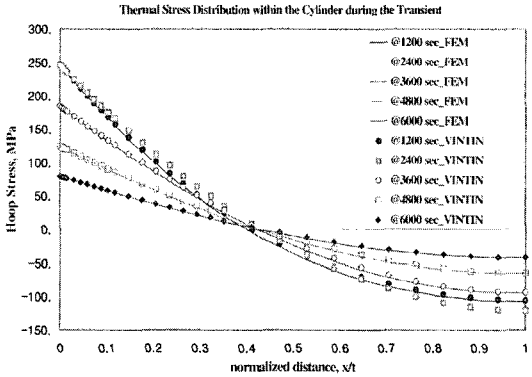


**Fig. 6** Comparison of the hoop stress distribution within the vessel at 1200, 2400, 3600, 4800 and 6000 seconds

#### 4.2.2 Influence coefficients

In Table 5, the influence coefficients approximated by VINTIN code are compared with those in the table in ASME Sec. XI App. A. As shown in the table, the influence coefficients in App. A are about 2 to 6% larger than those calculated by VINTIN code. It is not unusual because while VINTIN code uses the Raju-Newman's solution on the infinite cylinder with $t/R=0.1$, App. A values are derived from the analysis results on the infinite plate, or $t/R \rightarrow 0$, and conservatively applied for cylindrical geometry. Keeney also reported lower influence coefficients for flaws with $a/c=0.2$, but the difference were about 1% (Keeney and Bryson, 1995), less than what observed in this study.

#### 4.2.3 Stress intensity factors

The stress intensity factors at the tip of the 2/5 semi-elliptical flaws on the inner surface of the infinite cylinder at 1200, 2400, 3600, 4800, and 6000 seconds are summarized in Table 6. For SIF calculation using Raju-Newman method and ASME Sec. XI App. A method, stress distributions from FEM solution are fitted as the 3-rd order polynomials of distance normalized to flaw depth. For $a/t=0.2$ deep flaw, Raju-Newman method and VINTIN approximation result in fairly good agreement with the FEM solution using 1/4-symmetric flaw model. This point is also observed in internal pressure loading condition.

**Table 5** Comparison of the influence coefficients, $G_n$ for internal surface crack with $a/c=2/5$

| Case | $a/t$ | App. A | | | | VINTIN | | | |
|---|---|---|---|---|---|---|---|---|---|
| | | 0 | 1 | 2 | 3 | 0 | 1 | 2 | 3 |
| 2-1 | 0.05 | 1.0879 | 0.6833 | 0.5313 | 0.4482 | 1.0658 | 0.6656 | 0.5064 | 0.4207 |
| 2-2 | 0.1 | 1.0947 | 0.6855 | 0.5323 | 0.4488 | 1.0608 | 0.6660 | 0.5127 | 0.4293 |
| 2-3 | 0.2 | 1.1210 | 0.6939 | 0.5364 | 0.4511 | 1.0720 | 0.6720 | 0.5230 | 0.4410 |
| 2-4 | 0.25 | 1.1399 | 0.7000 | 0.5394 | 0.4528 | 1.0866 | 0.6773 | 0.5273 | 0.4448 |
| 2-5 | 0.4 | 1.2135 | 0.7249 | 0.5520 | 0.4605 | 1.1566 | 0.7013 | 0.5395 | 0.4519 |

Note : the VINTIN data for case 2)-3 are same as Raju-Newman's

Generally, ASME Sec. XI App. A method result in greater stress intensity factors than FEM solution and VINTIN approximation. The conservatism in ASME Sec. XI App. A that the influence coefficients are those for infinite plate rather than infinite cylinder can, in part, explain the results. This point is clear in Fig. 7 where the stress intensity factors from FEM solution and App. A are compared. The stress intensity factors from App. A method are 2-4% greater for $a/t=0.1$, and 5-10% greater for smaller and larger flaws. The difference become greater as the transient progresses.

The stress intensity factors from FEM solution and VINTIN approximation are compared in Fig. 8. As shown in the figure, the stress intensity factors from the VINTIN approximation are within $-0.1$-1.2% at $a/t=0.1$, and not greater than 6.3% for other flaw depths compared to those from FEM solution. When compared to the results for internal loading condition, the differences in the stress intensity factors become greater for cooldown transient condition. For $a/t=0.2$, the difference is 0.4% for internal pressure loading, but increases to 1.1-2.5% for cooldown transient. For deeper flaw, the difference become greater: it is 0.8% for $a/t=0.5$ under internal pressure loading, but it increases to 4.0-6.3% for $a/t=0.4$ under cooldown transient.

In approximating the stress intensity factors, the cooldown transient is different from the internal pressure loading condition. First, while the effects of the influence coefficient for constant stress term, $G_0$ is dominant for internal pressure loading condition (where stress profile is rather uniform along the thickness), those for the higher order stress terms, $G_1$, $G_2$, and $G_3$ become significant for cooldown transient condition. Second, because of the thermal stress variation along the thickness, polynomial approximation of the stress from the FEM solution could introduce some errors. Both of these contributes the increased

**Table 6** Comparison of the applied stress intensity factors calculated by various methods

| Case | $a/t$ | At 1200 Sec | | | | At 2400 Sec | | | | At 3600 Sec | | | | At 4800 Sec | | | | At 6000 Sec | | | |
|---|---|---|---|---|---|---|---|---|---|---|---|---|---|---|---|---|---|---|---|---|---|
| | | RN* | AS* | VIN | FE | RN* | AS* | VIN | FE | RN* | AS* | VIN | FE | RN* | AS* | VIN | FE | RN* | AS* | VIN | FE |
| 1 | 0.05 | | 38.34 | 37.64 | 36.71 | | 38.77 | 38.03 | 37.12 | | 29.12 | 28.55 | 27.78 | | 19.65 | 19.27 | 18.67 | | 12.61 | 12.36 | 11.92 |
| 2 | 0.1 | | 48.62 | 47.41 | 47.47 | | 49.84 | 48.55 | 48.53 | | 37.58 | 36.61 | 36.45 | | 25.41 | 24.75 | 24.55 | | 16.32 | 15.89 | 15.70 |
| 3 | 0.2 | 52.17 | 54.95 | 52.96 | 52.39 | 54.97 | 57.85 | 55.72 | 54.96 | 41.79 | 43.97 | 42.35 | 41.61 | 28.35 | 29.83 | 28.73 | 28.10 | 18.24 | 19.19 | 18.48 | 18.04 |
| 4 | 0.25 | | 54.67 | 52.63 | 51.69 | | 58.31 | 56.09 | 54.89 | | 44.48 | 42.78 | 41.71 | | 30.23 | 29.07 | 28.24 | | 19.46 | 18.71 | 18.13 |
| 5 | 0.4 | | 47.63 | 46.17 | 44.40 | | 52.49 | 50.90 | 48.52 | | 40.42 | 39.19 | 37.15 | | 27.57 | 26.73 | 25.23 | | 17.78 | 17.24 | 16.22 |

* Used stress distribution fitted using FEM results

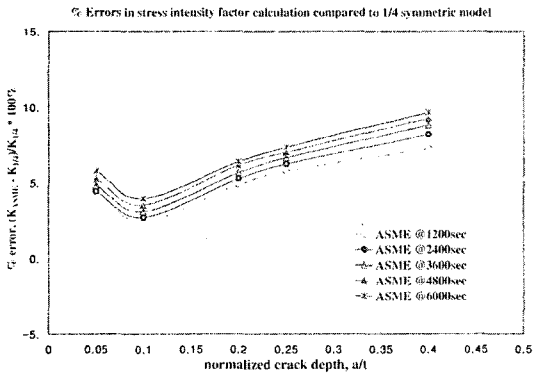


**Fig. 7** Percent difference in stress intensity factors, $(K_{ASME}-K_{1/1})/K_{1/4}*100\%$

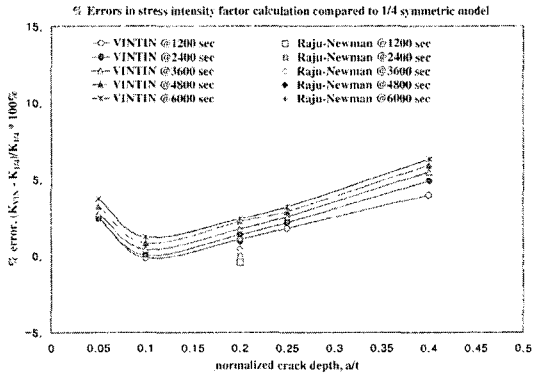


**Fig. 8** Percent difference in stress intensity factors, $(K_{VIN}-K_{1/4})/K_{1/4}*100\%$

errors in VINTIN approximation compared to FEM solution using 1/4-symmetric flaw model for cooldown transient.

### 4.3 VINTIN approximation for PTS transient

Above, we compared the approximation method to find the stress intensity factors with FEM solution for internal pressure loading and cooldown conditions separately. However, during the pressurized thermal shock transient that is the one of the key issues in reactor pressure vessels, stresses from both loading conditions are to be considered simultaneously to calculate the resulting stress intensity factors. In Fig. 9, the stress intensity factors at the tip of $a/t=0.2$ deep flaw from FEM solution using 1/4-symmetric flaw model and VINTIN approximation for PTS loading condition are compared. Throughout the period of the transient, both methods show good agreement in calculated stress intensity factors.

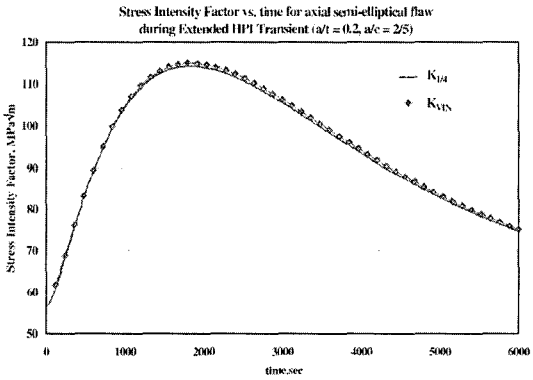


**Fig. 9** Comparison of stress intensity factor at the tip of semi-elliptical axial crack during the PTS transient

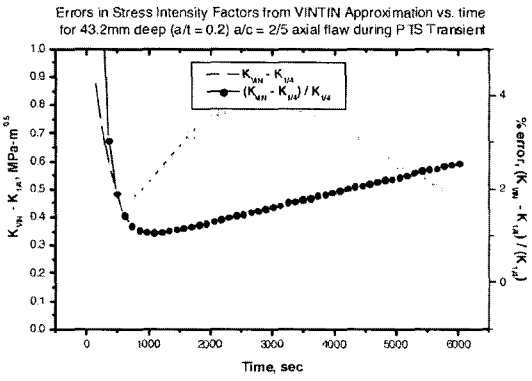


**Fig. 10** Differences between VINTIN approximation and 1/4 symmetric FEM solution of stress intensity factor at the tip of semi-elliptical axial crack during the PTS transient

In Fig. 10, errors in VINTIN approximation during the PTS transient are shown. Throughout the period of the transient, the stress intensity factors from VINTIN approximation are slightly greater than those from FEM solution. However, the errors are no more than 1 MPa$\sqrt{m}$. In percentage, that corresponds to about 2% except the very early stage of the transient. These degree of error are greater than that for internal pressure loading condition (about 0.4%) and less than those for cooldown condition (up to 2.5%). Though the errors are expected to increase for larger flaws due to increased errors in SIF from thermal stress, they are still less compared to ASME Sec. XI App. A method. Furthermore, for reasonably large flaws that are important in integrity assessment of the reactor pressure vessel in nuclear power plants, the errors in VINTIN approximation under combined loading of internal pressure and cooldown are expected to be less than 5%, which is reasonably good for approximation.

## 5. Conclusions

In this paper, a simple approximation method for the stress intensity factor at the tip of the axial semi-elliptical cracks on the cylindrical vessel is introduced. The approximation method, incorporated in VINTIN (Vessel INTegrity analysis-INner flaws), utilizes the influence coefficients to calculate the stress intensity factor at the crack tip. Also several other approximation methods to calculate the stress intensity factors at the tip of the semi-elliptical surface flaws in infinite cylinder. The approximation methods are compared with the 3-D finite element analysis for various flaw shapes and depths under loading conditions such as, internal pressure, cooldown, and pressurized thermal shock. Following conclusions are drawn from the results of the analysis.

(1) For the 1/8-symmetric flaw model, the calculated stress intensity factors in the present finite element analysis are 4-10% larger than those using the Raju-Newman's method.

(2) Instead, the calculated stress intensity factors using the 1/4-symmetric flaw model results in good agreement with those using the Raju-Newman's method, despite the Raju-Newman's method are based on the FEM analysis on the 1/8-symmetric flaw model.

(3) VINTIN approximation method in which the influence coefficients of Raju-Newman's method are used also shows good agreement with 3-D FEM analysis using the 1/4-symmetric flaw model.

- Under internal pressure loading condition, the calculated SIFs using VINTIN approximation are within $\pm 2.5\%$ of those from FEM analysis.

- Under cooldown condition, the differences in the calculated SIFs between the VINTIN approximation and the FEM analysis are $-0.1$-$1.2\%$ for $a/t=0.1$, then increase up to 6.3% for $a/t=0.4$.

(4) For the pressurized thermal shock transient condition, the stress intensity factors from VINTIN approximation are slightly greater than those from FEM solution. However, the errors are about 2% except the very early stage of the transient. These degree of error are greater than that for internal pressure loading condition and less than those for cooldown condition.

## References

ASME, 1995, Analysis of Flaws, ASME B&PV Code Sec. XI, App. A.

Dickson, T. L., 1994, FAVOR : A Fracture Analysis Code For Nuclear Reactor Pressure Vessels, Release 9401, ORNL/NRC/LTR/94/1.

Jang, C. H. et al., 2000, VINTIN : Vessel Integrity Analysis Inner Flaws, KEPRI Report TM. 00NP10.P2000.350.

Jang, C. H., Moonn, H. R., Jeong, I. S. and Hong, S. Y., 2001a, "Development of The Improved Probabilistic Fracture Mechanics Analysis Code : VINTIN," *In 2001 KNS Spring Meeting*, Cheju, Korea.

Jang, C. H., Moonn, H. R. and Jeong, I. S., 2001b, "Stress Intensity Factor Calculation For The Semi-Elliptical Surface Flaws On The Thin-Wall Cylinder Using Influence Coefficients," *In 2001 KSME Spring Meeting*, Cheju, Korea.

Keeney, J. A. and Bryson, J. W., 1995, "Stress Intensity Factor Influence Coefficients For Semi-elliptical Inner Surface Flaws In Clad Pressure Vessels," *Fracture Mechanics*, Vol. 26, pp. 430~443.

Kim, Y. J., Kim, H. G. and Im, S., 2001, "Mode Decomposition of Three-Dimensional Mixed-Mode Cracks Via Two-State Integrals," *Int. J. Solids and Structures*, Vol. 38, pp. 6405~6426.

Moonn, H. R. and Jang, C. H., 2001, "Comparison of Stress Intensity Factors For Longitudinal Semi-Elliptical Surface Cracks In Cylindrical Pressure Vessels," *In 2001 KSME Spring Meeting*, Cheju, Korea.

Raju, I. S. and Newman, J. C., 1982, "Stress Intensity For Internal Surface Cracks In Cylindrical Vessels," *ASME Journal of Pressure Vessel Technology*, Vol. 104, pp. 293~298.

Shih, C. F., Moran, B. and Nakamura, T., 1986, "Energy Release Rate Along A Three-Dimensional Crack Front In Thermally Stressed Body," *Int. J. of Fracture*, Vol. 30, pp. 79~102.

Simonen, F. A. et al., 1986, VISA-II A Computer Code For Predicting The Probability of Reactor Vessel Failure, NUREG/CR-4486.

Timoshenko, S., 1940, Theory of Plate and Shells, New York : McGraw-Hill.

USNRC, 1982, NRC Staff Evaluation of Pressurized Thermal Shock, SECY82-465.

Wang, X. and Lambert, S. B., 1996, "Stress Intensity Factors And Weight Functions For Longitudinal Semi-Elliptical Surface Cracks In Thin Pipes," *International Journal of Pressure Vessel & Piping*, Vol. 65, pp. 75~87.

Wu, X. and Carlsson, A. J., 1991, Weight Functions and Stress Intensity Factor Solutions, Oxford : Pergamon Press.